PNAS RESEARCH ARTICLE | ENGINEERING

Unbiased mechanical cloaks

Fernando Vasconcelos Senhora[a], Emily D. Sanders[b], and Glaucio H. Paulino[c,d,1]

Affiliations are included on p. 10.

Edited by Nader Engheta, University of Pennsylvania, Philadelphia, PA; received July 25, 2024; accepted January 23, 2025 by Editorial Board Member John A. Rogers

The distinction between "reinforcement" and "cloaking" has been overlooked in optimization-based design of devices intended to conceal a defect in an elastic medium. In the former, a so-called "cloak" is severely biased toward one or a few specific elastic disturbances, whereas in the latter, an "unbiased cloak" is effective under any elastic disturbance. We propose a two-stage approach for optimization-based design of elastostatic cloaks that targets true, unbiased cloaks. First, we perform load-case optimization to find a finite set of worst-case design loads. Then we perform topology optimization of the cloak microstructure under these worst-case loads using a judicious choice of the objective function, formulated in terms of energy mismatch. Although a small subset of the infinite load cases that the cloak must handle, these highly nonintuitive, worst-case loads lead to designs that approach perfect and unbiased elastostatic cloaking. In demonstration, we consider elastic media composed of spinodal architected materials, which provides an ideal testbed for exploring elastostatic cloaks in media with varying anisotropy and porosity, without sacrificing manufacturability. To numerically verify the universal nature of our cloaks, we compare the elastic response of the medium containing the cloaked defect to that of the undisturbed medium under many random load cases not considered during design. By using digital light processing additive manufacturing to realize the elastic media containing cloaked defects and analyzing their response experimentally using compression testing with digital image correlation, this study provides a physical demonstration of elastostatic cloaking of a three-dimensional defect in a three-dimensional medium.

elastostatic cloaking | structural optimization | architected materials

Invisibility has fascinated science fiction consumers throughout the ages and continues to be depicted in mainstream media as a superhuman ability or technology that remains millennia ahead of our time. Despite its fanciful portrayal, optical invisibility (and invisibility at other frequencies on the electromagnetic spectrum) was proven to not only be possible in theory via transformation cloaking (1, 2), but to also be physically achievable. The first electromagnetic cloak was composed of an assembly of microcircuit unit cells that rendered an object invisible to incident radiation at microwave frequencies (3). This ensemble of circuits was an early metamaterial example, or material exhibiting extraordinary properties beyond those attainable by traditional materials (4). Later, metamaterials capable of cloaking in optical frequencies were also demonstrated experimentally (5–7).

Mechanical cloaking is analogous to electromagnetic cloaking, but it applies to elastic fields rather than electromagnetic fields. The goal of mechanical cloaking is to manipulate the mechanical response of a material such that defects, e.g., voids or inclusions, are rendered mechanically invisible to their surroundings. Elastostatic cloaking focuses on invisibility with respect to the elastic response of a material subjected to static disturbances. Despite being less famous than its optical twin, elastostatic cloaking has a wide range of applications, e.g., tunnels that do not disturb surrounding buildings and geological formations; safer windows in aircraft, spacecraft, or submarines; and drug-delivery systems or health monitoring devices inserted into bone-tissue. However, when compared to their electromagnetic counterparts, the design of mechanical cloaks has proven to be challenging.

Initial efforts in design of elastostatic cloaks (8–11) were typically inspired by electromagnetic cloak design principles that rely on form-invariance of Maxwell's equations and make use of a coordinate transformation to arrive at a material-parameter distribution (e.g., distribution of electrical resistivity) that ensures cloaking. However, form invariance is lacking in the tensor-valued governing equations of elasticity and it has been proven mathematically that mechanical transformation cloaking is fundamentally

Significance

An elastostatic cloak conceals a defect from the material response to (quasi-)static mechanical stimuli under any elastic disturbance to the surrounding medium. Existing optimization-based design approaches severely bias their cloaks toward a few load cases, leading us to question their classification as elastostatic cloaks. We use several worst-case loading conditions to achieve unbiased cloaks that approach perfect cloaking and promote integrating engineered "defects" (e.g., tunnels that do not disturb surrounding buildings, safer windows in aircrafts) into materials without undesirable mechanical consequences under the uncertainties inherent in practice. By comparing our cloaks to microstructural patterns around tree knots, we ask whether nature designs elastostatic cloaks or favors biased reinforcement, and ponder how engineers may interpret optimality differently than nature does.

Author contributions: F.V.S., E.D.S., and G.H.P. designed research; F.V.S. performed research; F.V.S. analyzed data; and F.V.S., E.D.S., and G.H.P. wrote the paper.

The authors declare no competing interest.

This article is a PNAS Direct Submission. N.E. is a guest editor invited by the Editorial Board.

[1]To whom correspondence may be addressed. Email: gpaulino@princeton.edu.

This article contains supporting information online at https://www.pnas.org/lookup/suppl/doi:10.1073/pnas.2415056122/-/DCSupplemental.

Published May 9, 2025.

impossible in classical elasticity (12, 13). Nevertheless, it remains to be seen whether metamaterials can be designed using other methods to achieve perfect elastostatic cloaks.

This open question has prompted a push toward optimization-based design of elastostatic cloaks in recent years (14–18). One benefit of optimization-based cloaking over transformation cloaking is that optimization-based cloaks need not preserve the topology of the domain, i.e., additional holes can be introduced, which broadens the cloak design space. We too pursue an optimization-based approach to elastostatic cloak design, but in doing so, we emphasize a clear distinction between "unbiased elastostatic cloaking," in which the artifact is invisible under arbitrary elastic disturbances (12), and "reinforcement" (19), which may render a defect "neutral under one far-field load [but not] neutral under another one" (12). Cloaking is not the same as reinforcement; in fact, cloaking has important practical benefits over reinforcement. For example, under tractions and displacements not used in design, reinforcement can lead to stress concentrations that induce unwanted effects. In the case of bone integration, for instance, a discontinuity in the tissue elastic properties due to reinforcement can stimulate nerve endings, causing discomfort to the patient (20, 21). Unbiased elastostatic cloaking offers the potential to integrate engineered defects into a material without undesirable consequences on the static mechanical response of the system when subjected to the diversity of loading conditions experienced in practice.

The distinction between cloaking and reinforcement has become obscured in recent years as optimization formulations have been narrowly focused on using one or two load cases in design and only evaluating the ability to conceal a defect under those loads (14, 16, 17, 22–25). Although elastostatic cloaking in the continuum is not possible via transformation cloaking and the direct lattice transformation (DLT) approach has been acknowledged to only produce approximate elastostatic cloaks in lattice materials (9–11), DLT was shown to be significantly superior to optimization-based approaches that only design for one load case when evaluated for the ability to conceal the defect under some other load case (15). In fact, the insight underlying DLT, i.e., that global stiffness properties should be invariant under transformation between the domain with and without defect, is key to achieving perfect elastostatic cloaks that are not biased to a particular elastic disturbance. From an optimization perspective, one way to promote this invariance is to consider many load cases in design. Some elastostatic cloaks have been designed considering more than a few load cases during optimization, but the importance of this point is often overlooked and the performance under other elastic disturbances is often ignored (16). In fact, only a select few demonstrate that cloaks optimized for many load cases perform well for load cases not considered in design (15, 18). Nevertheless, these cloaks may still be severely biased due to their narrow focus on combinations of axial and shear loading conditions.

In an effort to reduce bias in optimization-based design of elastostatic cloaks and achieve "universal" cloaking performance, i.e., effectiveness under any arbitrary elastic disturbance, we determine load cases that pose the most difficulty in designing reinforcement to conceal the defect. We find that these worst-case loading scenarios are highly nonintuitive and by considering them during optimization-based design of the cloak, we significantly reduce the bias toward particular elastic disturbances and begin to approach perfect and universal elastostatic cloaks. While our cloaks are only approximate, we show that they have minor deviations from perfect performance using an energy mismatch metric that compares the response of the undisturbed surrounding elastic medium to that when the cloaked defect is present. Furthermore, by computing this energy mismatch for a large, but finite, number of arbitrary elastic disturbances (i.e., evaluation loads), we demonstrate universality of the designs. We emphasize that for practical applications, a close approximation of a perfect cloak can be as effective as the more elusive perfect cloak.

We also investigate how important a rich space of elastic properties is to achieving effective, universal, elastostatic cloaks by providing the optimization formulation with access to spinodal architected materials for which anisotropy and porosity can be locally tuned without sacrificing manufacturability (26, 27). While others argue that a diverse set of architected materials is critical to achieving effective elastostatic cloaking (16), we find that freedom in relative density of a given architecture is enough to achieve highly effective, universal, elastostatic cloaks that conceal defects of arbitrary geometry. The spinodal setting also provides a testbed where we can investigate how difficult it is to achieve universality in cloak performance as we vary the anisotropy and porosity of the surrounding elastic medium.

In addition to numerical validation of the universal nature of our elastostatic cloaks under 1,000 randomly selected evaluation load cases not considered during design, we also experimentally demonstrate their cloaking effectiveness under static compression (also not considered during design). Our elastostatic cloaks, manufactured using digital light processing (DLP) three-dimensional (3D) printing and verified using CT-scans, serve as a compelling physical demonstration of elastostatic cloaking of a 3D defect in a 3D medium.

Results

We start by introducing several domains needed to fully define the elastostatic cloaking design problem (Fig. 1). The ground truth domain refers to a stochastic volume element (SVE) taken from an infinite medium that is free from defects. The defect domain consists of the same SVE as the ground truth domain, but it includes a defect that we wish to hide. The cloak domain is the same as the defect domain, but includes a cloak design region around the defect where the optimizer is allowed to modify the material's microstructure to engineer the cloak. A probe region surrounds the cloak design region and is used to assess the cloak effectiveness by comparing its mechanical response to the response in the corresponding region of the ground truth domain (a similar comparison can also be made between the defect and ground truth domains). No alterations to the microstructure are allowed in the probe region of the cloak domain. Since the influence of the defect on mechanical behavior of the medium reduces with distance from the defect, the probe region does not need to extend far beyond the cloak design region; thus, the SVE size is dictated by the cloak design region size. With this terminology in place, the elastostatic cloaking problem is defined as follows: design the microstructure in the cloak design region to hide a defect so that the cloak domain and the ground truth domain have the same mechanical behavior, i.e., the same displacement field, in the probe region.

To quantify the difference in displacements in the probe region between the cloak and ground truth domains, we define the energy mismatch ($\mathcal{M}$),

$$\mathcal{M}(\widehat{\mathbf{u}}, \mathbf{u}, \mathbf{K}) = (\mathbf{u} - \widehat{\mathbf{u}})^T \mathbf{M}^T \mathbf{K} \mathbf{M} (\mathbf{u} - \widehat{\mathbf{u}}), \qquad [1]$$

based on quantities associated with the discretization used to approximate the solution of the governing equations of static elasticity of each system. In Eq. **1**, $\widehat{\mathbf{u}}$ is the vector of nodal displacements in the ground truth domain; $\mathbf{u}$ and $\mathbf{K}$ are the vector of nodal displacements and stiffness matrix, respectively, of the cloak domain; and $\mathbf{M}$ is an indicator matrix that nullifies contributions from degrees of freedom outside of the probe region (i.e., $M_{ij} = 0$ if $i \neq j$, $M_{ij} = 1$ if $i = j$ represents a degree of freedom inside the probe region, and $M_{ij} = 0$ if $i = j$ represents a degree of freedom outside the probe region). A similar energy mismatch, $\mathcal{M}(\widehat{\mathbf{u}}, \widetilde{\mathbf{u}}, \widetilde{\mathbf{K}})$, can be quantified for the defect domain by substituting its displacement vector, $\widetilde{\mathbf{u}}$, and stiffness matrix, $\widetilde{\mathbf{K}}$, into Eq. **1**. A successful cloaking design depends on the selection of an insightful objective function, and thus, these energy mismatches are used in the objective function for optimization-based design of the cloak. We use weighted least-squares, which are often used when portions of the data should be prioritized more than others (28). By including the stiffness matrix in the weighting matrix, $\mathbf{M}^T\mathbf{K}\mathbf{M}$, of the energy mismatch function, displacements associated with higher strain energies are prioritized in optimization and rigid body motions are disregarded (15).

The full procedure used to design elastostatic cloaks that effectively conceal the influence of a defect with arbitrary geometry under arbitrary elastic disturbances to the medium, is illustrated in Fig. 1 and detailed in *Materials and Methods*. We begin by using optimization to find a set of loading conditions that produce the largest energy mismatch in the defect domain and use them as design load cases in a subsequent topology optimization step for design of the cloak's microstructure. The objective function used for optimal design of the cloak consists of the sum of energy mismatch of the cloak domain over these worst-case design load cases, normalized by the sum of energy mismatch of the defect domain over the same load cases.

To provide flexibility in local design of the cloak microstructure, we equip the topology optimization formulation with architected materials, using spinodal materials, that can be tuned to achieve a wide range of mechanical properties. We adopt a multimaterial, spinodal topology optimization approach where the optimization can choose from four spinodal classes: isotropic, cubic (reinforced in three orthogonal directions), lamellar (resembling plate-like composites), and columnar (resembling fiber-like composites) (26). During topology optimization, the spinodal class, spinodal density,* and spinodal orientation are selected, locally, at each point of the cloak design region (27). For more details on spinodal architected materials, see *SI Appendix*, section 1.A.

In addition to enabling diversity of achievable material properties, spinodal architected materials promote manufacturability by facilitating seamless transitions between the different spinodal classes, densities, and orientations (26, 27). Thus, in a final step, the optimized cloak with spinodal embedded microstructures is manufactured using DLP 3D printing. We highlight that our structural optimization design approach for elastostatic cloaking is general and could be used with other classes of architected materials, which, given sufficient tunability and manufacturability, could also lead to effective elastostatic cloaks.

*Density for the porous spinodal architectures refers to the fraction of solid phase in an SVE. The admissible density range is limited to 0.3 to 0.7 to ensure practical manufacturability. Densities below 0.3 pose challenges related to material connectivity, while densities above 0.7 can result in enclosed voids that trap liquid resin during 3D printing (29, 30).

Cloaking an Arbitrarily Shaped Defect. We attempt to cloak a void defect in the shape of the Stanford bunny, embedded in an elastic medium composed of an isotropic spinodal architected material with 0.4 density (Fig. 2*A*). The defect is centered in a cubic SVE of the material and consumes 6% of the cube volume. A sphere with radius equal to 45% of the cube edge length is centered in the cube and the portion of the sphere surrounding the bunny defect serves as the cloak design region. The optimized elastostatic cloak design is shown in Fig. 2*B*, where we observe that the optimization elects to use the isotropic spinodal class everywhere in the cloak, but arrives at a highly complex density distribution with higher densities concentrated closer to the defect.

To visualize the optimized design load cases used in the cloak optimization problem, in Fig. 2*C* we display the deformed configuration of the ground truth domain caused by the six design load cases. We also compare the effect of these design loads cases on the ground truth, defect, and cloak domains by plotting cross-sections of their deformation profiles for each load case. We notice a near-perfect match between the deformed cross-sections of the ground truth and cloak domains, while the defect domain's deformation is distinct. As expected, the mismatch is more apparent for the first four design loads, whereas discrepancies for design loads five and six are more nuanced (due to the sequential optimization approach described in *Materials and Methods*—$\mathcal{M}$ is highest for the first load case and reduces with each subsequent load case).

We also simulate a compression test of the ground truth, defect, and cloak domains and compare their deformed configurations in Fig. 2*D*, where each colored section of the deformed cube represents one of the three domains. We emphasize that this simple compression evaluation load case was not considered during design of the cloak, yet the deformed configuration highlights a clear distinction between mechanical response of the defect domain and that of the cloak and ground truth domains, which match closely. We also plot the principal stress trajectories along a middle cross-section of the cube, parallel to the load direction, in Fig. 2*D*. These trajectories represent the main load path from the loads to the support region. The stress trajectories in the ground truth domain flow directly downward because their path is not obstructed by the defect. The stress trajectories in the defect and cloak domains both divert around the defect, but in the probe region, those in the cloak domain are better able to recover the load path observed in the ground truth domain.

To evaluate universality of cloaks designed using our approach (i.e., their ability to perform well under arbitrary elastic disturbances), we evaluate their performance under 1,000 random evaluation load cases using numerical simulation. Each random load case is composed of a random force with magnitude between −1 and 1 at each degree of freedom on the surface of the SVE. We use these 1,000 random load cases to compare performance of cloaks designed considering uniform loads that have commonly been used in optimization-based design of elastostatic cloaks (i.e., one compression load case, or a combination of one compression and one shear load case), and one, two, six, or eight optimized load cases.

In Fig. 2*E*, the average of the energy mismatch (Eq. **1**) for all 1,000 random evaluation load cases, normalized to the worst-case energy mismatch of the defect domain under these random loads, is quantified for each design. When the cloak is designed for one uniform compression load, the normalized average energy mismatch of the cloak domain is significantly higher than that of the defect domain because the design becomes overfitted for

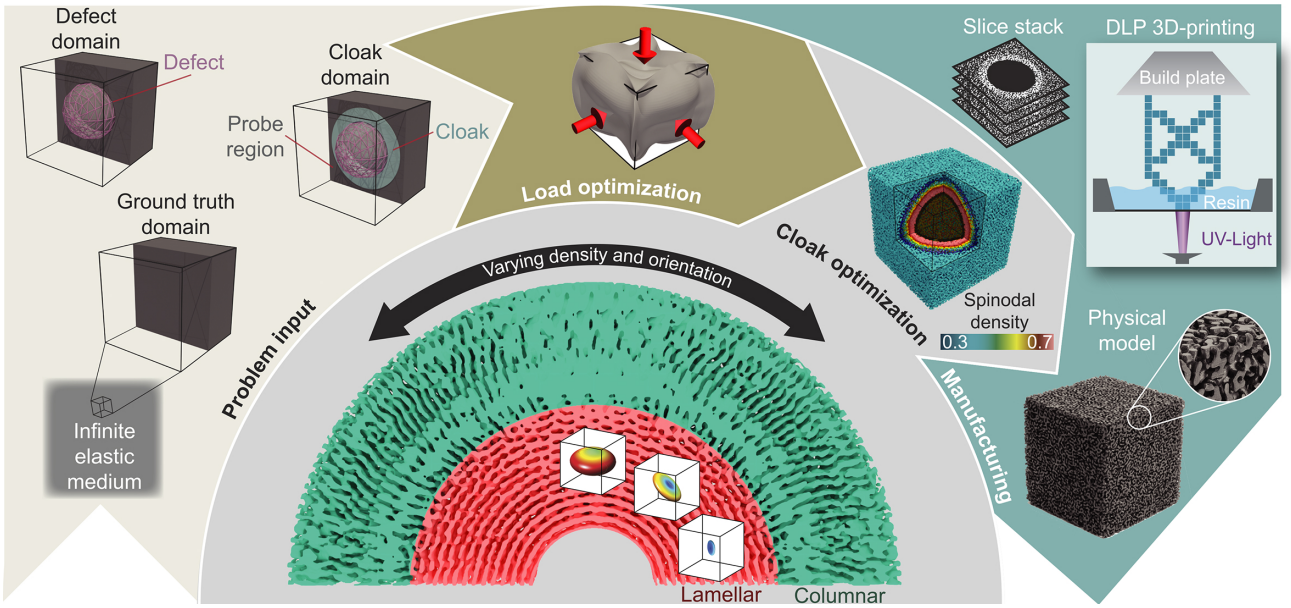

Fig. 1. Schematic of the spinodal cloaking design framework proposed in this work. We start by defining a ground truth and defect domain from a larger structure or infinite medium. At this stage, we also delimit the cloak and probe regions that we use to design and evaluate the cloak. Then, we optimize the load conditions to remove directional bias in the cloak performance. The optimized loads are used in the spinodal topology optimization procedure to design the cloak. The final cloak design is interpreted, and a slice-based approach is used to manufacture the computational model using Programmable PhotoPolymerization Digital Light Processing additive manufacturing.

one specific load case and, consequently, is unable to cloak the defect under other loads. Adding a uniform shear design load significantly improves the cloak's universality as evidenced by a drop in normalized average energy mismatch, but cloaks designed for the optimized load cases far surpass the performance of those designed with uniform loads even when only one optimized design load case is considered. As we increase the number of optimized design loads, we observe a clear trend of increased universality (i.e., the normalized average energy mismatch and its SD approach zero). Increasing the number of optimized design loads, however, increases the computational cost of the cloak optimization procedure because each load case requires a separate finite element analysis. Here, six design load cases provide a reasonable trade-off between cloak effectiveness and computational cost; thus, details and further analyses are provided for the cloak designed considering six optimized load cases.

We fabricated the ground truth, defect, and cloak domains using DLP 3D printing and verified the fidelity of the 3D printed structures relative to the computational models using measurements of cube height, width, length, and weight (*SI Appendix*, Table S1) and computed tomography scans (CT-scan). A comparison of the postprocessed CT-scan data and the expected geometry from the computational model revealed that printing errors only occurred in ≈1.4% of the total cube volume,[†] indicating that the physical models closely represent their idealized counterparts (Fig. 2*F*). For CT-scan results of the ground truth and defect domains, see *SI Appendix*, section 3.A.2 and Fig. S5.

To validate the computational and theoretical aspects of our results, we conducted mechanical experiments on the manufactured parts. Three repetitions (samples) of each domain class (ground truth, defect, and cloak) were evaluated under static compression testing, accompanied by 3D digital image correlation (DIC). The mean and envelope of the load-displacement curves for each domain class are provided in Fig. 2*G* (individual curves are provided in *SI Appendix*, Fig. S6) alongside load-displacement curves obtained from numerical simulation. The narrow envelopes of the load-displacement curves of each domain class indicates repeatable manufacturing. The slightly greater variations observed for the cloak domain's mechanical response are attributed to its more intricate microstructure that causes a higher degree of print errors (*SI Appendix*, Fig. S5). Strong agreement is also evident between the simulated and experimental load-displacement behavior.

Fig. 2*G* also shows y-displacement fields on one face of the cubes obtained using 3D DIC (x- y- and z-displacement fields of all samples are displayed in *SI Appendix*, Fig. S7). The DIC displacement fields clearly highlight the similarity between the mechanical response of the ground truth and cloak domains and the distinct mechanical response of the defect domain. To quantify how different the DIC displacement fields are between the different experimental samples, we use the mean absolute difference (MAD),

$$\mathrm{MAD}(\mathbf{U}_i, \mathbf{U}_j) = \frac{1}{N}\sum_{\ell=1}^{N} \left\| \mathbf{U}_i\left(x_\ell, y_\ell\right) - \mathbf{U}_j\left(x_\ell, y_\ell\right) \right\|_2, \qquad [2]$$

in which $\mathbf{U}_i$ and $\mathbf{U}_j$ are the DIC displacement fields of samples i and j, respectively; N is the total number of DIC displacement data points; and (x_ℓ, y_ℓ) is the coordinate of the ℓ^{th} DIC displacement data point. The MAD values, normalized to the highest MAD value, are listed in Table 1, where we observe low MAD values when comparing samples of the same domain class and when comparing samples from the ground truth and cloak domain classes. Conversely, higher MAD values are observed when comparing samples from the defect and cloak domain classes or defect and ground truth domain classes, as expected. The MAD values provide further evidence that the cloak domain exhibits mechanical behavior similar to that of the ground truth (i.e., the cloak design effectively conceals the bunny defect) and the defect domain's mechanical behavior is distinct.

[†]The total absolute volume of defects is the sum of volumes associated with extra and missing material.

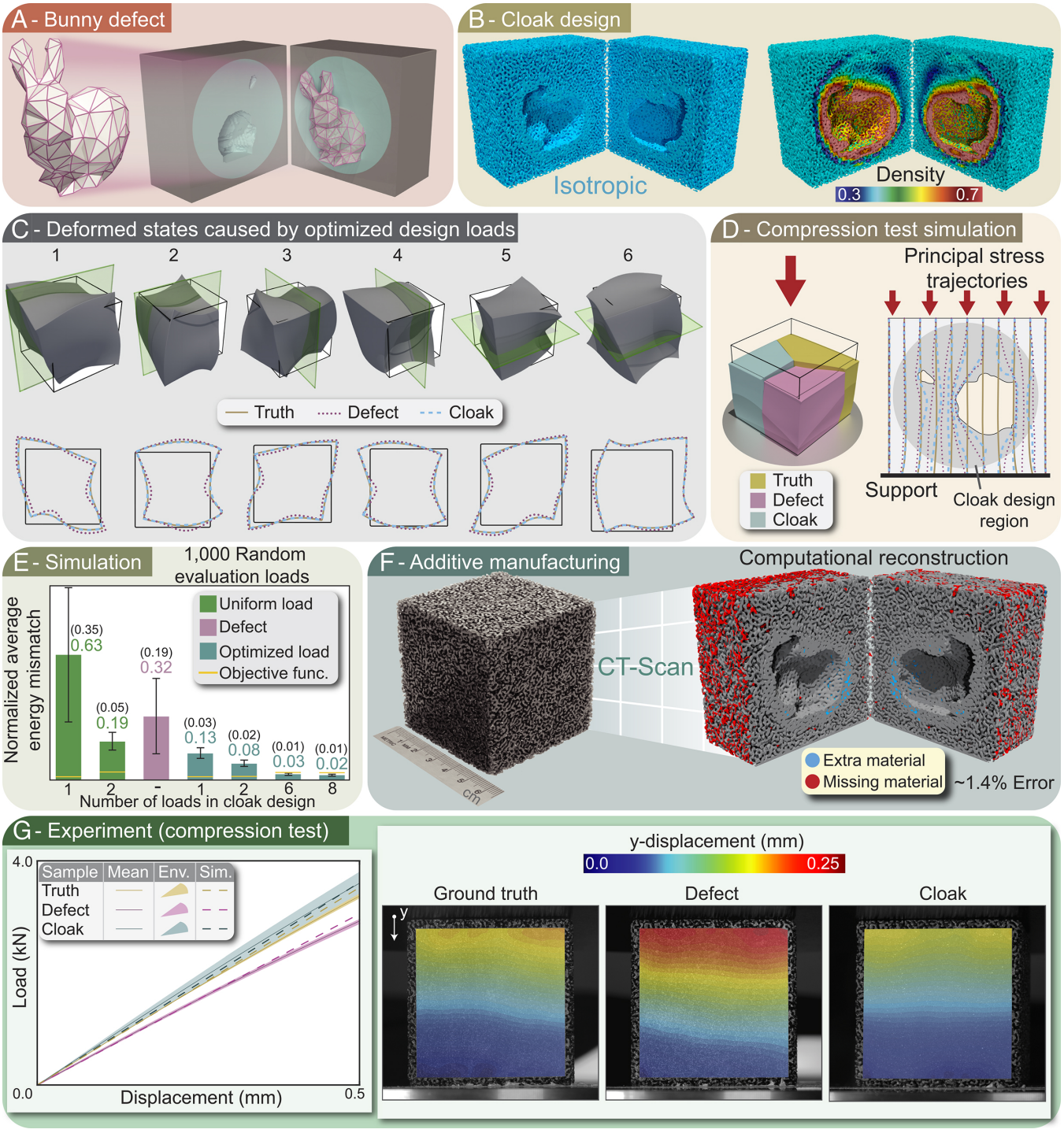

Fig. 2. Cloaking a void defect in the shape of the Stanford bunny embedded in an isotropic spinodal elastic medium with 0.4 density. (*A*) Schematic showing the Stanford Bunny defect geometry and cloak design region in blue. (*B*) Optimized cloak design, which contains only the isotropic spinodal class with a highly complex distribution of spinodal density. (*C*) Deformed configuration of the ground truth domain caused by the six optimized load cases used in the cloak design (*Top*) and cross-sections of the deformation profiles in the ground truth, defect, and cloak domains subjected to the six optimized load cases (*Bottom*). (*D*) Results of simulated compression tests of the ground truth, defect, and cloak domains, comparing their deformed shape and principal stress trajectories through a middle cross-section parallel to the load direction. (*E*) Average of the energy mismatch associated with 1,000 random evaluation load cases in numerical simulations of the defect domain and cloak domain (with several cloak designs), normalized to the worst-case energy mismatch of the defect domain (numbers within parenthesis represent SD). (*F*) Additively manufactured part and its reconstructed counterpart obtained from CT-scan data. (*G*) Results of experimental compression tests performed on the 3D printed models, including load-displacement plots and y-displacement fields obtained through 3D DIC.

Varying the Surrounding Elastic Medium. To evaluate the versatility and highlight limitations of our optimization-based approach to designing unbiased elastostatic cloaks, we vary the elastic medium in which the Stanford bunny (void) defect is embedded. First, we hold the spinodal class constant and vary the spinodal density (i.e., we consider an isotropic spinodal elastic medium, and in addition to 0.4 density, we consider 0.3, 0.5, 0.6, and 0.7 densities). Next, we hold the spinodal density constant

Table 1. Stanford bunny defect in a 0.4-density isotropic spinodal elastic medium: Mean absolute difference (MAD) of the 3D DIC displacement fields obtained from compression testing of additively manufactured specimens of the ground truth, defect, and cloak domains (three samples of each domain class)

		Normalized mean absolute difference (MAD)								
		Truth			Defect			Cloak		
Class	Sample	1	2	3	4	5	6	7	8	9
Truth	1	–								
	2	0.13	–							
	3	0.22	0.22	–						
Defect	4	0.66	0.70	0.62	–					
	5	0.77	0.78	0.72	0.35	–				
	6	0.75	0.75	0.72	0.09	0.35	–			
Cloak	7	0.28	0.26	0.38	0.76	0.73	1.00	–		
	8	0.25	0.25	0.27	0.73	0.70	0.99	0.11	–	
	9	0.22	0.18	0.34	0.74	0.70	0.95	0.35	0.36	–

Numbers below 0.5 (in black) indicate similar mechanical behavior and numbers above 0.5 (in red) indicate distinct mechanical behavior.

and vary the spinodal class (i.e., in addition to isotropic spinodal, we consider cubic, lamellar, and columnar spinodal elastic media with 0.4 density).

Varying the spinodal density of the elastic medium. Since a void defect reduces the stiffness of the material, the cloak must compensate by adding stiffer material than what is in the surrounding medium. Thus, we expect cloaking to be more challenging as density of the elastic medium increases. This hypothesis is supported in Fig. 3 *A–D*, where we see that as the density of the surrounding elastic medium increases, the amount of high-density material in the cloak design increases, until the 0.6 case, in which almost the whole cloak region is filled with the highest-density material (0.7). The normalized average energy mismatch of the designs based on 1,000 random evaluation loads (Fig. 3*E*) indicates that universal cloak performance peaks for 0.4 density and quickly degenerates as density of the surrounding elastic medium increases. This study indicates that a key requirement for effective elastostatic cloak design to conceal a void is that the design space contains materials that are significantly stiffer than that of the surrounding elastic medium. Material that is less stiff than the surrounding medium seems to provide little benefit to cloak performance, as the optimizer can introduce voids that play the role of the less stiff material.

Varying the spinodal class of the elastic medium. Cloaks designed to conceal the Stanford bunny (void) defect in elastic media composed of the cubic, lamellar, and columnar spinodal architected materials with 0.4 density are shown in Fig. 3 *F–H*. Similarly to the isotropic case, the optimizer only makes use of the spinodal class present in the surrounding elastic medium and the density tends to be higher close to the defect. Nevertheless, the spinodal density maps display subtle differences between the cloak designs for each spinodal material class. The normalized average energy mismatch of the designs based on 1,000 random evaluation loads (Fig. 3*I*) indicates that universality of cloaks designed for the lamellar spinodal elastic medium is significantly worse than that of cloaks designed for the other spinodal classes. The magnitude of the normalized average energy mismatch seems to be directly correlated with the degree of anisotropy (DoA)[‡] of the surrounding elastic medium (DoA for isotropic, cubic, lamellar, and columnar are 1.0, 1.3, 7.9, and 2.8, respectively) and we conjecture that DoA is an indicator of how difficult it is to design a universal elastostatic cloak in a given anisotropic medium. Nevertheless, we can improve universality of the cloak designs in the case of high DoA by increasing the number of optimized load cases used in design or increasing the material design space. The former approach reduces the normalized average energy mismatch from 0.16 ± 0.07 to 0.07 ± 0.02 when we increase from six to twelve optimized loads, at the cost of higher computational burden. The latter approach may introduce manufacturability challenges that need to be overcome.

In summary, this study indicates that density, rather than material architecture, is the controlling variable for an effective cloak design.

Do Trees Cloak Their Knots? Nature has demonstrated extreme resourcefulness time and again as mechanics-driven laws of growth have promoted optimal form in biological organisms (31, 32). Trees are an awe-inspiring example, in which a strong and resilient natural material (i.e., wood) enable trees to grow taller than any other known biological structure.

Wood has also shaped the course of human history (33), and to this day, is one of the most used construction materials (34, 35). Nevertheless, natural defects are known to be detrimental to mechanical properties needed for wood's engineering applications. For example, knots (Fig. 4 *A–C*), or portions of branches embedded in a tree's trunk wood, significantly reduce tensile and bending capacity of harvested wood (36, 37). A knot can be described as a cylindrical or conical defect extending radially outward from the trunk's interior (Fig. 4*C*). The inner portion of the knot forms while the branch is still alive, and thus, is intergrown with the trunk. The hard and dense nature of intergrown knots relative to the surrounding trunk wood leads to differential shrinkage and stress concentrations in harvested timber containing these inclusions. The outer portion of the knot is associated with the part of the branch that becomes encased in the trunk after the branch dies, but before it falls off. Encased knots are not mechanically integrated with the trunk and often lead to voids in harvested wood (38, 39). Both types of defects are detrimental to mechanical properties needed for engineering applications.

So how do trees overcome the potential negative impact of knots on their wood's mechanical properties to foster continued growth during their lifespan? Does a tree design its microstructure around knots to promote resilience to these defects? If so, is elastostatic cloaking at play or is reinforcement specific to

[‡]Here, degree of anisotropy is defined as the ratio of stiffness in the stiffest to least stiff directions of the material.

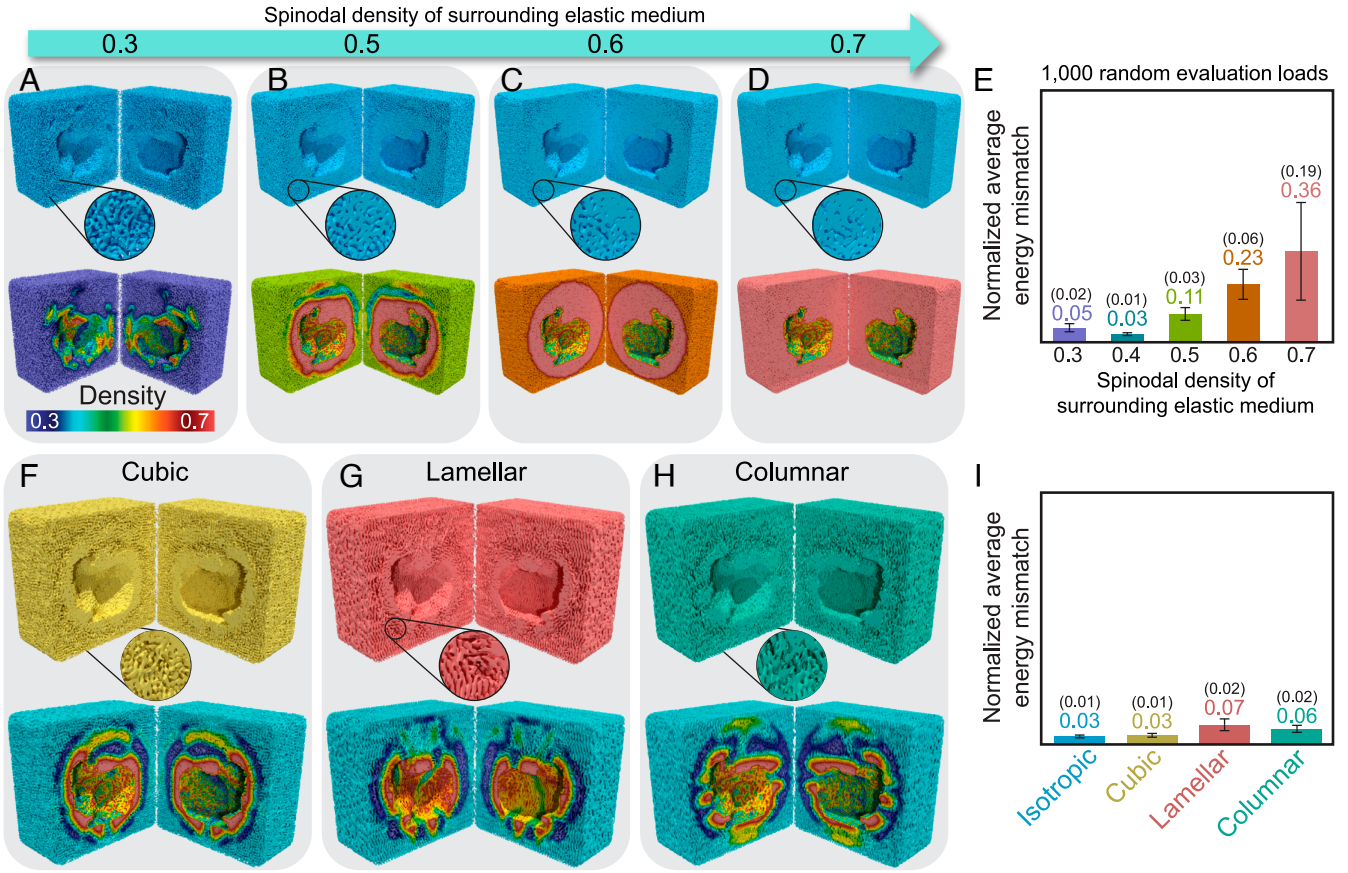

Fig. 3. Cloaking a void defect in the shape of the Stanford bunny embedded in elastic media with varying spinodal density and spinodal class. (*A*–*D*) Cloak designs for an isotropic elastic medium with 0.3, 0.5, 0.6, and 0.7 density, respectively (the design for 0.4 density are displayed in Fig. 2*B*). (*E*) Quantification of universal cloak performance as a function of density of the surrounding elastic medium using the normalized average energy mismatch associated with 1,000 random evaluation load cases via numerical simulations (numbers within parenthesis represent SD). (*F*–*H*) Cloak designs for cubic, lamellar, and columnar elastic media, respectively, with 0.4 density. (*I*) Quantification of universal cloak performance as a function of spinodal class in the surrounding elastic medium using the normalized average energy mismatch associated with 1,000 random evaluation load cases via numerical simulations (numbers within parenthesis represent SD).

the trunk's (mainly) compressive service loads more efficient? Although we do not attempt to fully answer these questions here, we use our computational framework for elastostatic cloak design to inspire further exploration along these lines. We define a lamellar spinodal elastic medium (with 0.3 density) reminiscent of a trunk's wood microstructure, embed a cylindrical void defect reminiscent of an encased knot, design a cloak around the knot, and compare the patterns in the cloak's design to those observed around knots in natural wood. The cloak domain for this problem is shown in Fig. 4*B*. The resulting cloak's lamella alignment is visualized and compared with a wood knot fiber orientation in front view in Fig. 4*C*, where we observe a clear resemblance between the wood knot and the cloak design. Fig. 4*D* shows cross-sectional views of the cloak design. The resemblance is less obvious in cross-section, possibly due to differences in the lamellar elastic medium used in the elastostatic cloak design and the tree's trunk wood microstructure. The full spinodal microstructure and spinodal density are displayed in Fig. 4*E*.

Discussion

Our research introduces an optimization-based approach to design universal elastostatic cloaks that can conceal disturbances due to arbitrarily shaped defects in 3D elastic media composed of spinodal architected materials. Unlike traditional cloaking methods that predominantly rely on combinations of tension, compression, and shear boundary conditions (14, 16, 17, 22–25), we preoptimize the boundary conditions used in optimization-based design of the elastostatic cloaks to eliminate (human) bias and promote universal cloaks that are effective under a diverse set of, often uncertain, loads encountered in real-world scenarios. Performance of the optimized cloaks was rigorously evaluated against 1,000 random loading conditions not used in design, demonstrating their robustness and universality.

By studying the effectiveness of the optimized cloaks as a function of the material composing the surrounding elastic medium, we concluded that an essential aspect of the material design space is to include both a candidate material with similar mechanical properties (e.g., isotropic or orthotropic), and a material significantly stiffer than the surrounding. Additionally, we observed that the degree of anisotropy impacts the performance of the universal cloak: The greater the anisotropy of the surrounding elastic medium, the more challenging it becomes to effectively cloak the defect.

A critical aspect of our work is in translating digital cloak designs into physical reality. Using DLP 3D printing, we produced 3D models of the cloak designs to showcase a practical means of materializing complex, microstructured designs. The manufactured samples were analyzed using CT-scans to ensure that the physical cloaks closely aligned with their idealized com-

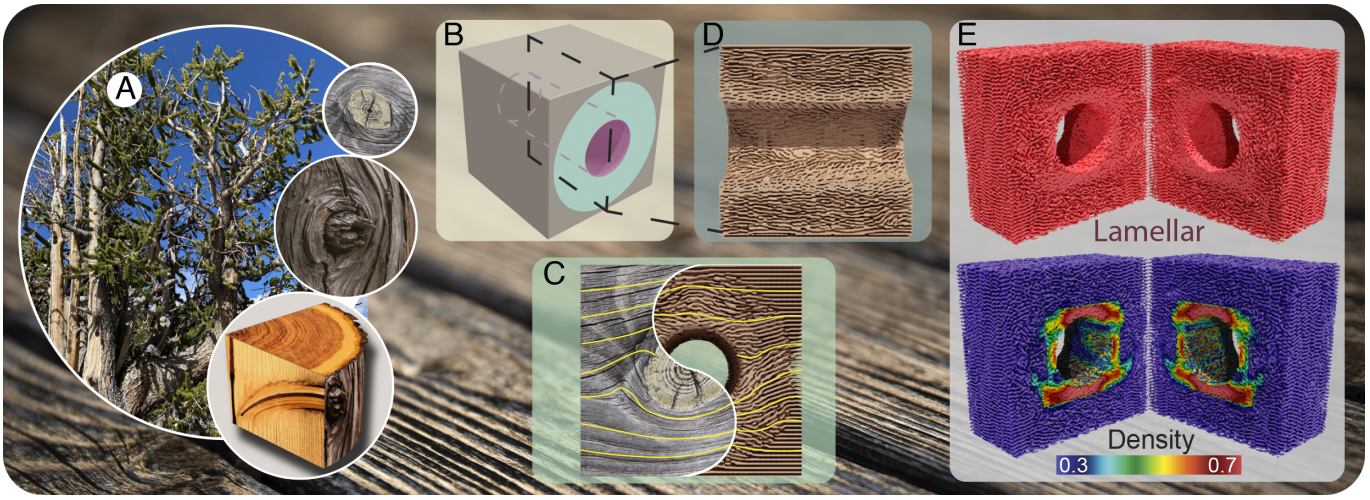

Fig. 4. Biomimicry of a wood knot through elastostatic cloaking (*A*) Bristlecone pine and wood knot examples (middle wood knot by cobalt123, Pine Tree Knot, CC BY-NC 2.0 DEED). (*B*) Design domain of the cloak displaying the cylindrical defect (purple) and the cloaking region (blue). (*C*) Comparison between a wood knot fiber and lamella orientation of an optimized cloak. (*D*) Side view of the lamella orientation of an optimized cloak. (*E*) Optimized cloak design embedded with spinodal microstructure using lamellar spinodal material and the spinodal density distribution of the design.

putational counterparts. Spinodal architected materials played a critical role in this effort as they enabled continuous variations in material properties, while maintaining manufacturability, without the need for extreme or unattainable properties (14, 18). Mechanical testing was used to verify the physical effectiveness of the cloaks and underline the physical feasibility of our method beyond the 2D domain that has dominated thought in cloaking research (14–16, 18, 23–25). In addition to the Stanford bunny defect, we also provide numerical and experimental results for a spherical defect (*SI Appendix*, section 3.B). Furthermore, by designing a cloak to conceal an idealized wood knot, we use elastostatic cloaking to pose an intriguing question regarding the meaning of optimality in nature versus engineering.

While our cloaks do not perfectly suppress the effect of the defect under all possible elastic disturbances, this limitation is a consequence of fundamental trade-offs between cloak effectiveness and practical considerations, i.e., attainable material properties, manufacturability, and whether a perfect cloak is possible at all. By focusing on approximate cloaks that perform well across a range of elastic disturbances and that can be manufactured using current technologies, we bring elastostatic cloak design closer to practical applications.

Building upon the results shown in this work, the transition from laboratory experiments to real-world implementation remains a critical step. One of the challenges will be adjusting the stiffness of the cloak to its surrounding medium. By selecting appropriate base materials for the spinodal microstructure, we can tune the cloak's stiffness to approximate that of its environment. With spinodal densities between 30% and 70%, we achieve stiffness values ranging from approximately 4% to 55% of the base material, which offers significant tunability. Our findings suggest that stiffness levels at least two to four times higher than the surrounding medium are crucial for effective cloaking. If the surrounding material has a very high stiffness, cloaking becomes more challenging, not due to limitations of the spinodal material itself, but as a general property of mechanical cloaking problems.

Collaborations with industry and interdisciplinary efforts will be pivotal in harnessing the potential of elastostatic cloaking across various domains. In fact, elastostatic cloaking is a first step toward more complex cloaking problems such as elastodynamic or acoustic cloaking. The techniques developed in this work can serve as a baseline for these and other future developments. Furthermore, we hope that this work highlights the difference between simple reinforcement, tailored to single or a limited number of load cases, and universal cloaking that aims to mimic the defect-free elastic medium for any elastic disturbance. We also emphasize the importance of choosing a material design space for the cloak design problem that takes into account manufacturability requirements.

Materials and Methods

Topology Optimization. The mathematical optimization statement of the elastostatic cloak design problem is defined as,

$$\begin{aligned}
\min_{\boldsymbol{\omega}\in\Omega} \quad & f(\boldsymbol{\omega}) = \frac{\sum_{i=1}^{n} \mathcal{M}(\widehat{\mathbf{u}}^{(i)}, \mathbf{u}^{(i)}(\boldsymbol{\omega}), \mathbf{K})}{\sum_{i=1}^{n} \mathcal{M}(\widehat{\mathbf{u}}^{(i)}, \widetilde{\mathbf{u}}^{(i)}, \widetilde{\mathbf{K}})} \\
\text{s.t.} \quad & g_{\ell j} = 4z_{\ell j}(1 - z_{\ell j}) + \sum_{p=1,\, p\neq j}^{m} 8 z_{\ell j} z_{\ell p} \leq 0, \\
& \ell = 1, \ldots, N^e,\ j = 1, \ldots, m \\
\text{with} \quad & \mathbf{K}(\boldsymbol{\omega})\,\mathbf{u}^{(i)}(\boldsymbol{\omega}) = \mathbf{F}^{(i)},\ i = 1, \ldots, n \\
& \widehat{\mathbf{K}}\widehat{\mathbf{u}}^{(i)} = \mathbf{F}^{(i)} \\
& \widetilde{\mathbf{K}}\widetilde{\mathbf{u}}^{(i)} = \mathbf{F}^{(i)}.
\end{aligned} \qquad [3]$$

In Eq. **3**, the set of cloak design variables, $\boldsymbol{\omega} = \{\mathbf{Z}, \boldsymbol{\rho}, \boldsymbol{\alpha}, \boldsymbol{\beta}, \boldsymbol{\gamma}\}$, contains the $N^e \times m$ matrix of spinodal selection design variables, $\mathbf{Z}$, which control the presence or absence of each of the m candidate spinodal classes at each of the N^e elements of the discretized cloak design region; the $N^e \times 1$ vector of density design variables, $\boldsymbol{\rho}$, which control the local spinodal density at each of the N^e elements; and the $N^e \times 1$ vectors of orientation design variables, $\boldsymbol{\alpha}$, $\boldsymbol{\beta}$, $\boldsymbol{\gamma}$, which control the local rotation of the spinodal microstructures at each of the N^e elements. Bounds on each component of $\mathbf{Z}$ are 0 and 1; bounds on each component of $\boldsymbol{\rho}$ are 0.3 and 0.7 (based on manufacturability requirements); and bounds on each component of $\boldsymbol{\alpha}$, $\boldsymbol{\beta}$, $\boldsymbol{\gamma}$, are $-\pi$ and π (modular arithmetic is used to ensure the orientation variables can move directly from π to $-\pi$). The objective function, $f(\boldsymbol{\omega})$, is a measure of how different the displacement

fields between the cloak and ground truth domains are in the probe region according to the energy mismatch, $\mathcal{M}$, defined in Eq. **1**. The inputs, $\widehat{\mathbf{u}}^{(i)}$, $\widetilde{\mathbf{u}}^{(i)}$, and $\mathbf{u}^{(i)}$, to the $\mathcal{M}$ function, are displacement fields of the ground truth, defect, and cloak domains, respectively, which are obtained by solving the discretized state equations associated with each domain, $\widehat{\mathbf{K}}\widehat{\mathbf{u}}^{(i)} = \mathbf{F}^{(i)}$, $\widetilde{\mathbf{K}}\widetilde{\mathbf{u}}^{(i)} = \mathbf{F}^{(i)}$, and $\mathbf{K}(\boldsymbol{\omega})\,\mathbf{u}^{(i)}(\boldsymbol{\omega}) = \mathbf{F}^{(i)}$ for the $i = 1, \ldots, n$ optimized design load cases, $\mathbf{F}^{(i)}$.

To translate the design variables into mechanical properties of the cloak design region, we adopt a material interpolation function that combines the solid isotropic material with penalization (SIMP) (40, 41) and discrete material optimization (DMO) (42, 43) functions such that the local constitutive tensor (in matrix notation) in element ℓ is given by,

$$\mathbf{D}_\ell = \sum_{j=1}^{m} (y_{\ell j})^p \prod_{\substack{k=1 \\ k\neq j}}^{m} \left[1 - \tilde{\gamma}(y_{\ell k})^p\right] \mathbf{R}\mathbf{D}_j^H(\rho_\ell)\,\mathbf{R}^T, \qquad [4]$$

where $p > 1$ is the SIMP penalty parameter, $0 < \tilde{\gamma} \leq 1$ the spinodal mixing penalty parameter, $\mathbf{D}_j^H(\rho_\ell)$, is the homogenized constitutive tensor (in matrix notation) of spinodal class j that varies as a function of the spinodal density (27), and $\mathbf{R}(\alpha_\ell, \beta_\ell, \gamma_\ell)$ is a matrix that performs the fourth-order tensor rotation (in matrix notation) dictated by the spinodal orientation design variables. In Eq. **4**, $y_{\ell j}$, is obtained from the spinodal selection design variables in $\mathbf{Z}$, by first applying a density filter that imposes a minimum macroscale feature size (44, 45), and then a smooth Heaviside projection operator that projects intermediate values to their 0/1 bounds (46, 47). The Heaviside projection is defined as,

$$y_{\ell j} = \frac{\tanh(\xi\eta) + \tanh(\xi(P_{\ell i} z_{ij} - \eta))}{\tanh(\xi\eta) + \tanh(\xi(1-\eta))}, \qquad [5]$$

where $\eta = 0.5$ is the Heaviside's threshold parameter, $0.1 \leq \xi \leq 15$ controls the steepness of the Heaviside function, and the filter matrix is,

$$P_{\ell i} = \frac{h_{\ell i} A_i}{\sum_{k=1}^{N^e} h_{\ell k} A_k}, \quad h_{\ell i} = \max\left[0, (r - ||\mathbf{x}_\ell - \mathbf{x}_i||_2)\right], \qquad [6]$$

where A_i is the volume of element i, $\mathbf{x}_\ell$ and $\mathbf{x}_i$ are the coordinates of elements ℓ and i, respectively, and r is the filter radius.

The SIMP and DMO interpolation functions used in Eq. **4** are effective in penalizing intermediate values of the spinodal selection design variables and preventing mixing of the different spinodal classes when the optimization problem involves a tradeoff between stiffness and volume, but they are not as effective for the current elastostatic cloaking formulation. To force a 0/1 spinodal selection distribution without mixing, we introduce local constraints, $g_{\ell j}$, $\ell = 1, \ldots, N^e$, $j = 1, \ldots, m$, that make it so that the only feasible choices of $z_{\ell 1}, \ldots, z_{\ell m}$ in element ℓ are cases in which $z_{\ell i} = 1$ and $z_{\ell j} = 0\,\forall j \neq i$. The constraint functions and associated feasible region for element ℓ of a fictitious two-spinodal material case is displayed in *SI Appendix*, Fig. S2. The combination of the constraints with the SIMP and DMO penalizations helps the optimizer to avoid unfavorable local optima and achieve meaningful solid-void solutions.

To handle the local constraints in the optimization problem of Eq. **3**, we use the augmented Lagrangian (AL) method (48, 49), which substitutes the problem's constraints with a penalty term in the objective function (for more details on AL for topology optimization, see ref. 50). In addition to handling many local constraints, an advantage of the AL method is that it does not impose feasibility at every optimization step, meaning that the optimizer can transverse infeasible regions of the design space to reach optimal points that are otherwise inaccessible, while guaranteeing feasibility at convergence.

Elastostatic Cloak Design Boundary Conditions. The boundary conditions imposed on the ground truth, defect, and cloak domains, which enter into the state equations used in the topology optimization formulation of Eq. **3**, play a pivotal role in the resulting cloak's universality. We use a combination of Neumann and Robin boundary conditions,

$$\begin{array}{ll} \text{Neumann} & \text{Robin} \\ (\boldsymbol{\sigma}\cdot\mathbf{n})|_{\partial\Omega} = \mathbf{t}^0 & (\boldsymbol{\sigma}\cdot\mathbf{n} + \mathbf{k}\mathbf{u})|_{\partial\Omega} = \mathbf{t}^0, \end{array} \qquad [7]$$

to represent the design load cases and the effect of the surrounding infinite medium, respectively. In Eq. **7**, $\boldsymbol{\sigma}$ is the continuous stress field, $\mathbf{n}$ is a unit vector normal to the domain boundary, $\partial\Omega$, $\mathbf{t}^0$ is the prescribed boundary tractions, $\mathbf{k}$ represents stiffness of Hookean springs, and $\mathbf{u}$ is the continuous displacement field. The spring stiffness is empirically set to 0.01 of the maximum component of the ground truth domain stiffness matrix.

To design a perfect universal cloak, i.e., a cloak that effectively conceals a defect from any elastic disturbance, all possible boundary tractions should be considered in the design process (i.e., number of load cases, $n \to \infty$); however, considering an infinite number of load cases is computationally infeasible. Instead, we uniquely tailor a finite number of boundary tractions that, when used in design, lead to cloaks within some tolerance of perfect universal elastostatic cloaking. To remove human bias in defining the load cases, we use optimization to find the load cases that maximize the energy mismatch associated with the defect, i.e., we aim to find the "hardest" loads to conceal effectively. This load case optimization problem is mathematically expressed as,

$$\begin{aligned} \min_{\mathbf{F}^{(i)}, \cdots, \mathbf{F}^{(n)}} \quad & \mathcal{F} = -\sum_{i=1}^{n} \mathcal{M}\left(\widehat{\mathbf{u}}^{(i)}\left(\bar{\mathbf{F}}^{(i)}\right), \widetilde{\mathbf{u}}^{(i)}\left(\bar{\mathbf{F}}^{(i)}\right), \widetilde{\mathbf{K}}\right) \\ \text{s.t.} \quad & h_{ij} = \left[\left(\bar{\mathbf{F}}^{(i)}\right)^T \bar{\mathbf{F}}^{(j)}\right]^2 - \delta_{ij} - \epsilon(1-\delta_{ij}) \leq 0, \\ & \qquad i, j = 1, \ldots, n \\ \text{with} \quad & \widehat{\mathbf{K}}\widehat{\mathbf{u}}^{(i)} = \bar{\mathbf{F}}^{(i)} \quad i = 1, \ldots, n \\ & \widetilde{\mathbf{K}}\widetilde{\mathbf{u}}^{(i)} = \bar{\mathbf{F}}^{(i)} \\ & \bar{\mathbf{F}}^{(i)} = \bar{\mathbf{P}}\mathbf{F}^{(i)}, \end{aligned} \qquad [8]$$

where the optimization variables are the load vectors associated with the discretized state equations, $\mathbf{F}^{(i)}, \cdots, \mathbf{F}^{(n)}$, which are restricted to the surface of the domain (i.e., no load is allowed inside of the domain). The constraints, h_{ij}, impose orthonormality to the load vectors, $\mathbf{F}^{(i), i=1,\ldots,n}$, and allow us to obtain a variety of diverse loading conditions (the term $\epsilon(1-\delta_{ij})$ allows for a small degree $\epsilon = 0.01$ of nonorthogonality to the loads). The matrix $\bar{\mathbf{P}}$ in Eq. **8** is a filter, similar to $\mathbf{P}$ in Eq. **6**, that smooths the load variable, $\mathbf{F}^{(i)}$, to obtain the effective load $\bar{\mathbf{F}}^{(i)}$, but unlike $\mathbf{P}$, $\bar{\mathbf{P}}$ acts separately on each of the load components (x, y, and z), and it is only defined on the surface of the domain (i.e., its output $\bar{\mathbf{F}}^{(i)}$ is still restricted to the domain surface).

Solving for all $\mathbf{F}^{(i)}$, $i = 1, \ldots, n$, concurrently leads to instability in the load optimization problem. To improve stability, we solve for each of the $i = 1, \ldots, n$ load vectors sequentially. That is, instead of solving one optimization problem with $\mathbf{F}^{(i)}, \ldots, \mathbf{F}^{(n)}$ design variables, we solve n optimization problems, each for a single load vector. While solving the i^{th} optimization problem, we only impose the h_{ij} constraints with $j \leq i$, in which the $\mathbf{F}^{(j)}$, $j < i$, are the load vectors found in the previous optimization problems. By having the constraints associated with fixed, previously optimized, $\mathbf{F}^{(j)}$, $j < i$ vectors, the optimizer can effortlessly achieve feasibility. Conversely, optimizing all loads simultaneously can cause them to adversely compete for the same optimal point, resulting in instability in the optimization procedure. Furthermore, the sequential optimization of the loads allows us to easily scale up or down the number of loads without having to rerun the full load optimization problem. We solve the optimization problem in Eq. **8** and feed the optimized load vectors to the cloak design optimization problem of Eq. **3**. It is noted that the optimized load cases are dependent on both the defect that we wish to cloak and the elastic medium in which the defect is embedded.

Elastostatic Cloak Validation. From the cloak design optimization, we obtain a map of spinodal class, density, and orientation in the cloak design region. These maps are interpreted to generate the microstructure embedded cloak design by taking a level-set of a Gaussian random field that defines the spinodal geometry

(*SI Appendix*, section 1.A) (27, 30, 51). The level-set function, which acts as a local indicator for the presence or absence of material, is queried to generate a stack of 2D slices, or images representing cross-sections of the 3D model. Each pixel of the 2D slices corresponds to a voxel in the 3D space and its value indicates the presence or absence of material. The slices are sent to the DLP 3D printer, which exposes a UV-sensitive resin to UV light according to the patterns in the 2D pixelated slices, to solidify the resin layer-by-layer into the shape of the 3D part. By using a slice-based printing technique, we do not need to directly generate a full 3D model (e.g., STL file), which can be prohibitively memory-consuming and hard to postprocess in traditional 3D printing software due to the incredibly detailed microstructure-embedded parts of interest here.

Following this slicing procedure, we manufacture ground truth, defect, and cloak domain samples for the Stanford bunny defect embedded in an isotropic spinodal elastic medium with 0.4 density. The samples are subjected to a strict postprocessing protocol to obtain repeatable and consistent material properties (*SI Appendix*, section 2.C and Fig. S3). The samples are analyzed using CT-scans to verify that the geometrical features of the fabricated samples closely match those of the computational models (*SI Appendix*, section 2.D). The postprocessed samples are subjected to a compression test in which we measure global force and displacement and compute local displacement fields using 3D DIC. More details about the manufacturing and experiments can be found in *SI Appendix*, section 2.

Data, Materials, and Software Availability. The computer code supporting the findings of this study is openly available at Zenodo (52). All other data are included in the article and/or supporting information.

ACKNOWLEDGMENTS. We acknowledge the NSF under grants CMMI-2105811 and CMMI-2323415.

Author affiliations: [a]School of Civil and Environmental Engineering, Georgia Institute of Technology, Atlanta, GA 30332; [b]George W. Woodruff School of Mechanical Engineering, Georgia Institute of Technology, Atlanta, GA 30332; [c]Department of Civil and Environmental Engineering, Princeton University, Princeton, NJ 08544; and [d]Princeton Materials Institute, Princeton University, Princeton, NJ 08544

1. J. B. Pendry, D. Schurig, D. R. Smith, Controlling electromagnetic fields. *Science* **312**, 1780–1782 (2006).
2. U. Leonhardt, Optical conformal mapping. *Science* **312**, 1777–1780 (2006).
3. D. Schurig *et al*., Metamaterial electromagnetic cloak at microwave frequencies. *Science* **314**, 977–980 (2006).
4. D. R. Smith, J. B. Pendry, Homogenization of metamaterials by field averaging. *JOSA B* **23**, 391–403 (2006).
5. J. Valentine, J. Li, T. Zentgraf, G. Bartal, X. Zhang, An optical cloak made of dielectrics. *Nat. Mater.* **8**, 568–571 (2009).
6. L. H. Gabrielli, J. Cardenas, C. B. Poitras, M. Lipson, Silicon nanostructure cloak operating at optical frequencies. *Nat. Photon.* **3**, 461–463 (2009).
7. T. Ergin, N. Stenger, P. Brenner, J. B. Pendry, M. Wegener, Three-dimensional invisibility cloak at optical wavelengths. *Science* **328**, 337–339 (2010).
8. T. Bückmann, M. Thiel, M. Kadic, R. Schittny, M. Wegener, An elasto-mechanical unfeelability cloak made of pentamode metamaterials. *Nat. Commun.* **5**, 4130 (2014).
9. T. Bückmann, M. Kadic, R. Schittny, M. Wegener, Mechanical cloak design by direct lattice transformation. *Proc. Natl. Acad. Sci. U.S.A.* **112**, 4930–4934 (2015).
10. L. Hai, Q. Zhao, Y. Meng, Unfeelable mechanical cloak based on proportional parameter transform in bimode structures. *Adv. Funct. Mater.* **28**, 1801473 (2018).
11. M. Kadic *et al*., Elastodynamic behavior of mechanical cloaks designed by direct lattice transformations. *Wave Motion* **92**, 102419 (2020).
12. A. Yavari, A. Golgoon, Nonlinear and linear elastodynamic transformation cloaking. *Arch. Ration. Mech. Anal.* **234**, 211–316 (2019).
13. A. Golgoon, A. Yavari, Transformation cloaking in elastic plates. *J. Nonlinear Sci.* **31**, 1–76 (2021).
14. V. D. Fachinotti, I. Peralta, A. E. Albanesi, Optimization-based design of an elastostatic cloaking device. *Sci. Rep.* **8**, 9857 (2018).
15. E. Sanders, M. Aguiló, G. Paulino, Optimized lattice-based metamaterials for elastostatic cloaking. *Proc. R. Soc. A* **477**, 20210418 (2021).
16. L. Wang *et al*., Mechanical cloak via data-driven aperiodic metamaterial design. *Proc. Natl. Acad. Sci. U.S.A.* **119**, e2122185119 (2022).
17. Y. Lu, L. Tong, Concurrent multiscale topology optimization of metamaterials for mechanical cloak. *Comput. Methods Appl. Mech. Eng.* **409**, 115966 (2023).
18. F. Sozio, M. F. Shojaei, A. Yavari, Optimal elastostatic cloaks. *J. Mech. Phys. Solids* **176**, 105306 (2023).
19. E. H. Mansfield, Neutral holes in plane sheet-reinforced holes which are elastically equivalent to the uncut sheet. *Q. J. Mech. Appl. Mech.* **6**, 370–378 (1953).
20. K. S. Topp, B. S. Boyd, Structure and biomechanics of peripheral nerves: Nerve responses to physical stresses and implications for physical therapist practice. *Phys. Ther.* **86**, 92–109 (2006).
21. A. Alzaharani *et al*., The innervation of the human acetabular labrum and hip joint: An anatomic study. *BMC Musculoskelet. Disord.* **15**, 1–8 (2014).
22. J. C. Á. Hostos, V. D. Fachinotti, I. Peralta, Metamaterial for elastostatic cloaking under thermal gradients. *Sci. Rep.* **9**, 1–9 (2019).
23. X. Cheng *et al*., A compatible boundary condition-based topology optimization paradigm for static mechanical cloak design. *Extreme Mech. Lett.* **65**, 102100 (2023).
24. Y. Jia, K. Liu, X. S. Zhang, Topology optimization of irregular multiscale structures with tunable responses using a virtual growth rule. *Comput. Methods Appl. Mech. Eng.* **425**, 116864 (2024).
25. Y. Jia, K. Liu, X. S. Zhang, Unstructured growth of irregular architectures for optimized metastructures. *J. Mech. Phys. Solids* **192**, 105787 (2024).
26. S. Kumar, S. Tan, L. Zheng, D. M. Kochmann, Inverse-designed spinodoid metamaterials. *NPJ Comput. Mater.* **6**, 1–10 (2020).
27. F. V. Senhora, E. D. Sanders, G. H. Paulino, Optimally-tailored spinodal architected materials for multiscale design and manufacturing. *Adv. Mater.* **34**, 2109304 (2022).
28. Y. Bard, *Nonlinear Parameter Estimation* (Academic Press, New York, NY, 1974).
29. A. Vidyasagar, S. Krödel, D. M. Kochmann, Microstructural patterns with tunable mechanical anisotropy obtained by simulating anisotropic spinodal decomposition. *Proc. R. Soc. A Math. Phys. Eng. Sci.* **474**, 20180535 (2018).
30. C. Soyarslan, S. Bargmann, M. Pradas, J. Weissmüller, 3D stochastic bicontinuous microstructures: Generation, topology and elasticity. *Acta Mater.* **149**, 326–340 (2018).
31. D. W. Thompson, *On Growth and Form* (Cambridge University Press, UK, ed. 1, 1917).
32. C. Darwin, *On the Origin of Species by Means of Natural Selection, or Preservation of Favoured Races in the Struggle for Life* (John Murray, London, 1859).
33. J. Glausiusz, Wood-the vein that runs through human history. *Nature* **588**, 26–27 (2020).
34. M. H. Ramage *et al*., The wood from the trees: The use of timber in construction. *Renew. Sustain. Energy Rev.* **68**, 333–359 (2017).
35. H. E. Ilgın, M. Karjalainen, O. P. Koponen, A. Soikkeli, "A study on contractors' perception of using wood for construction" in *Engineered Wood Products for Construction*, M. Gong, Ed. (IntechOpen, 2022), p. 97.
36. IO for Standardization (ISO), *Sawn Timber of Broadleaved Species - Defects - Terms and Definitions ISO 2300:1973* (Wiley, New York, 1973).
37. S. J. Record, *The Mechanical Properties of Wood* (Wiley, New York, 1914).
38. E. Rapraeger, Development of branches and knots in western white pine. *J. For.* **37**, 239–245 (1939).
39. P. Hoffmeyer, "The role of grain angle, knots, tension wood, compression wood, and other anomalies on the mechanical properties of wood," Ph.D. thesis, Technical University of Denmark, Lyngby, Denmark (1987).
40. M. Zhou, G. Rozvany, The COC algorithm, part II: Topological, geometrical and generalized shape optimization. *Comput. Methods Appl. Mech. Eng.* **89**, 309–336 (1991).
41. M. P. Bendsøe, Optimal shape design as a material distribution problem. *Struct. Optim.* **1**, 193–202 (1989).
42. J. Stegmann, E. Lund, Discrete material optimization of general composite shell structures. *Int. J. Numer. Meth. Eng.* **62**, 2009–2027 (2005).
43. E. D. Sanders, A. Pereira, M. A. Aguiló, G. H. Paulino, Polymat: An efficient Matlab code for multi-material topology optimization. *Struct. Multidiscip. Optim.* **58**, 2727–2759 (2018).
44. B. Bourdin, Filters in topology optimization. *Int. J. Numer. Meth. Eng.* **50**, 2143–2158 (2001).
45. T. Borrvall, J. Petersson, Topology optimization using regularized intermediate density control. *Comput. Methods Appl. Mech. Eng.* **190**, 4911–4928 (2001).
46. J. K. Guest, J. H. Prévost, T. Belytschko, Achieving minimum length scale in topology optimization using nodal design variables and projection functions. *Int. J. Numer. Meth. Eng.* **61**, 238–254 (2004).
47. F. Wang, B. S. Lazarov, O. Sigmund, On projection methods, convergence and robust formulations in topology optimization. *Struct. Multidiscip. Optim.* **43**, 767–784 (2011).
48. D. P. Bertsekas, *Nonlinear Programming* (Athena Scientific, ed. 2, 1999).
49. J. Nocedal, S. Wright, *Numerical Optimization* (Springer Science & Business Media, 2006).
50. F. V. Senhora, O. Giraldo-Londono, I. F. Menezes, G. H. Paulino, Topology optimization with local stress constraints: A stress aggregation-free approach. *Struct. Multidiscip. Optim.* **62**, 1639–1668 (2020).
51. J. W. Cahn, Phase separation by spinodal decomposition in isotropic systems. *J. Chem. Phys.* **42**, 93–99 (1965).
52. G. H. Paulino *et al*., Unbiased mechanical cloaks. Zenodo. https://doi.org/10.5281/zenodo.15271218. Deposited 23 April 2024.